ANTIOXIDANTS & REDOX SIGNALING
Volume 36, Numbers 7–9, 2022

DOI: 10.1089/ars.2021.0047

ORIGINAL RESEARCH COMMUNICATION

Renal NOXA1/NOX1 Signaling Regulates Epithelial Sodium Channel and Sodium Retention in Angiotensin II-induced Hypertension

Aleksandr E. Vendrov,[1] Mark D. Stevenson,[1] Andrey Lozhkin,[1] Takayuki Hayami,[1] Nathan A. Holland,[2] Xi Yang,[2] Nicholas Moss,[2] Hua Pan,[3] Samuel A. Wickline,[3] James D. Stockand,[4] Marschall S. Runge,[1] Nageswara R. Madamanchi,[1,*] and William J. Arendshorst[2,*]

Abstract

Aims: NADPH oxidase (NOX)-derived reactive oxygen species (ROS) are implicated in the pathophysiology of hypertension in chronic kidney disease patients. Genetic deletion of NOX activator 1 (*Noxa1*) subunit of NOX1 decreases ROS under pathophysiological conditions. Here, we investigated the role of NOXA1-dependent NOX1 activity in the pathogenesis of angiotensin II (Ang II)-induced hypertension (AIH) and possible involvement of abnormal renal function.

Results: NOXA1 is present in epithelial cells of Henle's thick ascending limb and distal nephron. Telemetry showed lower basal systolic blood pressure (BP) in *Noxa1*$^{-/-}$ *versus* wild-type mice. Ang II infusion for 1 and 14 days increased NOXA1/NOX1 expression and ROS in kidney of male but not female wild-type mice. Mean BP increased 30 mmHg in wild-type males, with smaller increases in *Noxa1*-deficient males and wild-type or *Noxa1*$^{-/-}$ females. In response to an acute salt load, Na^+ excretion was similar in wild-type and *Noxa1*$^{-/-}$ mice before and 14 days after Ang II infusion. However, Na^+ excretion was delayed after 1–2 days of Ang II in male wild-type *versus Noxa1*$^{-/-}$ mice. Ang II increased epithelial Na^+ channel (ENaC) levels and activation in the collecting duct principal epithelial cells of wild-type but not *Noxa1*$^{-/-}$ mice. Aldosterone induced ROS levels and *Noxa1* and *Scnn1a* expression and ENaC activity in a mouse renal epithelial cell line, responses abolished by *Noxa1* small-interfering RNA.

Innovation and Conclusion: Ang II activation of renal NOXA1/NOX1-dependent ROS enhances tubular ENaC expression and Na^+ reabsorption, leading to increased BP. Attenuation of AIH in females is attributed to weaker NOXA1/NOX1-dependent ROS signaling and efficient natriuresis. *Antioxid. Redox Signal*. 36, 550–566.

[1]Division of Cardiovascular Medicine, Department of Internal Medicine, University of Michigan, Ann Arbor, Michigan, USA.
[2]Department of Cell Biology and Physiology, University of North Carolina, Chapel Hill, North Carolina, USA.
[3]Department of Cardiovascular Sciences, University of South Florida, Tampa, Florida, USA.
[4]Department of Cellular and Integrative Physiology, University of Texas Health Science Centre at San Antonio, San Antonio, Texas, USA.
*Both authors are joint senior authors.

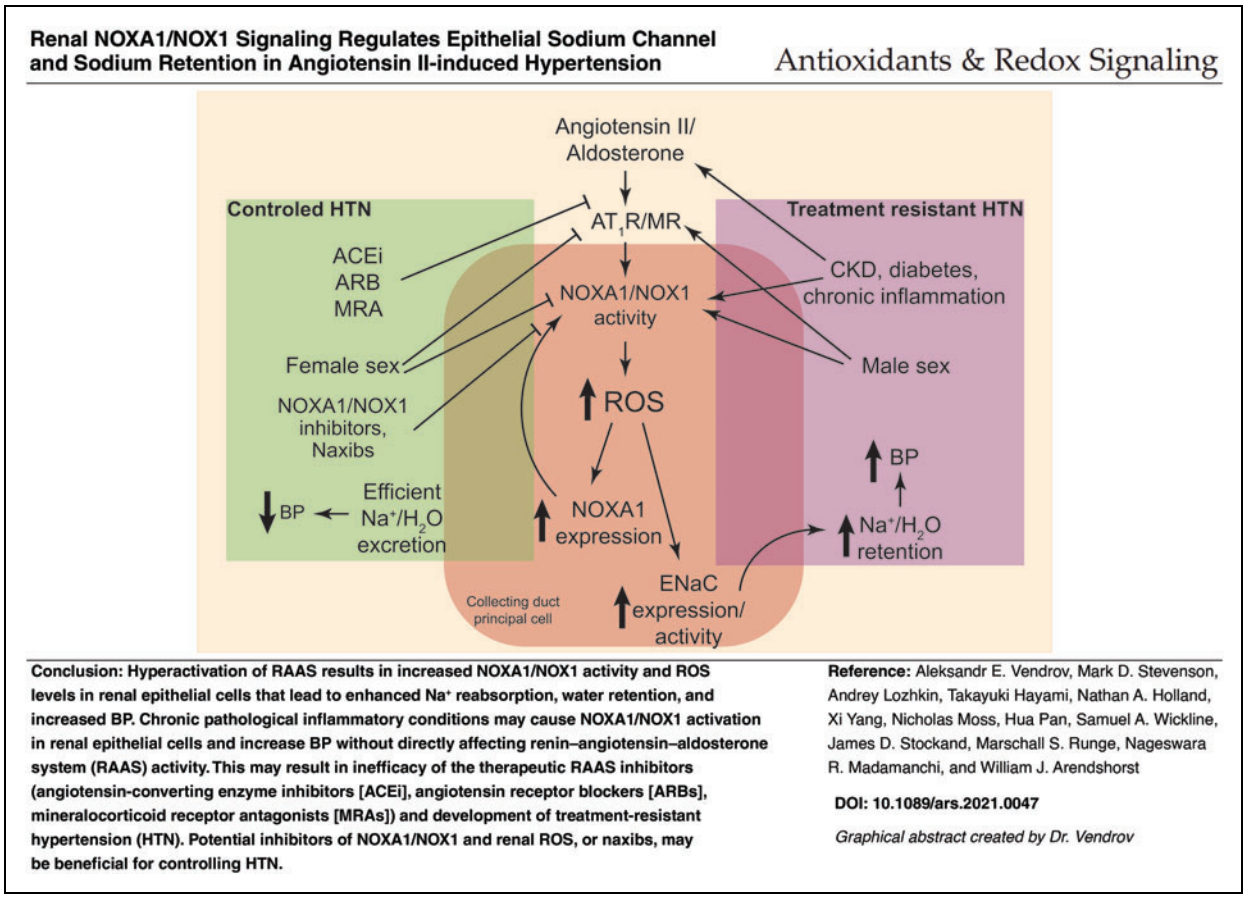

Color images are available online.

Keywords: reactive oxygen species, hypertension, kidney, epithelial sodium channels, sex difference, tubular epithelial cells

Introduction

Chronic kidney disease (CKD) and hypertension (HTN) have intermingled cause and effect relationships (23), and are among the major risk factors for cardiovascular diseases (55). Nearly 40% of CKD patients develop apparent treatment-resistant HTN where optimal levels of blood pressure (BP) are not achieved with use of three different classes of medications (51). This underscores the complexity of HTN pathophysiology with many of pathogenic factors and the need for the development of new therapeutic strategies.

Hyperactivation of the renin–angiotensin–aldosterone system (RAAS) causes vasoconstriction, reduces filtered Na^+ load, and increases tubular Na^+ reabsorption, favoring Na^+ retention and HTN by shifting the pressure–natriuresis relation to a higher BP (18). Exaggerated renal vasoconstriction and Na^+ retention often result from an imbalance of the natriuretic vasodilator $^{\bullet}NO$ and the antinatriuretic vasoconstrictor superoxide anion ($O_2^{\bullet-}$) (12, 26).

Increased reactive oxygen species (ROS) generation may be a key integrating factor coupling angiotensin II (Ang II)-induced activation of RAAS to the reduced Na^+ excretion, vasoconstriction, and inflammation (28). The resultant renal dysfunction likely initiates a self-perpetuating process, inducing and maintaining HTN. Excessive Na^+ and volume retention are common characteristics of treatment-resistant HTN (22).

In the vasculature, NADPH oxidases (NOXs) are the main sources of ROS resulting from Ang II/Ang II type 1 (AT_1) receptor activation (39). A number of NOX catalytic subunits—NOX1, NOX2, and NOX4—are expressed in the

Innovation

NOX activator 1 (NOXA1)-dependent NADPH oxidase plays a critical role in mediating renin–angiotensin–aldosterone system hyperactivation and hypertension (HTN). Here, we discovered that NOXA1 is expressed in renal tubular epithelial cells, and mediates angiotensin II (Ang II)-induced activation of renal NOX1 and reactive oxygen species (ROS) levels. Genetic deletion of *Noxa1* reduces basal and Ang II-induced HTN with more efficient Na^+ excretion early during Ang II infusion in association with decreased renal ROS and epithelial Na^+ channel expression and activity. Lower expression of NOXA1 correlates with attenuated renal ROS levels, higher Na^+ excretion, and lower blood pressure in Ang II-induced hypertension (AIH) in female *versus* male mice. Targeting NOXA1 in AIH in combination with traditional therapy is an attractive, promising strategy.

renal vasculature, glomerular and tubular structures (17, 29). Activation of NOX1 requires interaction of membrane-bound NOX1 and p22phox with cytosolic regulatory subunits p47phox, p67phox, and Rac1, which are in turn activated in response to agonists or injury.

Alternatively, NOX1 can interact with p47phox homolog NOXO1 and p67phox homolog NOX activator 1 (NOXA1), causing constitutive production of $O_2^{\bullet-}$ (49). In mouse vascular smooth muscle cells (VSMCs), NOXA1 is required for NOX1 activation, whereas NOX1 is activated by binding with p67phox in endothelial cells (1). We previously demonstrated that NOXA1 interacts with p47phox in VSMC and is a critical component of NOX1 activation regulating vascular function and inflammation (41, 54).

Ang II infusion induces ROS generation and eNOS uncoupling in the vasculature, primarily through activation of NOX1 (37, 44). In addition, Ang II increases the expression of NOX1 in vascular and renal cells (37, 59) and NOXA1 in the vasculature (41). Congruent with such responses, genetic deletion of NOX1 attenuates vascular $O_2^{\bullet-}$ production, restores endothelial function, and reduces the magnitude of Ang II-induced hypertension (AIH) (16, 35). On the contrary, mice overexpressing NOX1 in VSMC display a more pronounced AIH (13). In contrast, BP regulation in a chronic HTN mouse model is independent of NOXs and oxidative stress (61). NOX1 may contribute to diabetic nephropathy, promote glomerular hypertrophy, mesangial fibrosis, podocyte loss, and albuminuria (45).

The epithelial Na^+ channel (ENaC) is a key transporter that fine tunes Na^+ reabsorption in the distal nephron, primarily in collecting duct (CD) principal cells. Enhanced Na^+ reabsorption *via* increased ENaC activity causes volume expansion and HTN (6, 14). NOX-derived ROS in general and NOX4 were implicated in Ang II stimulation of ENaC activity in *ex vivo* studies of distal nephrons and CD cell lines, respectively (31, 32). However, little is known about NOXA1/NOX1 signaling in renal function in HTN, and there is no evidence to date linking NOXA1 or NOX1 to renal vascular or tubular abnormalities in AIH.

Our studies characterize NOXA1-dependent NOX1 expression and activity and downstream signaling pathways involving ROS in the mouse kidney during basal conditions and the development and maintenance phases of AIH. A causal relationship to abnormal renal function is suggested by an early phase of delayed Na^+ excretion during initial development of AIH in wild-type males, with normal Na^+ excretion during established HTN. Genetic deletion of *Noxa1* reduced renal ROS production, normalized Na^+ excretion during the developmental phase of HTN, and attenuated the development and magnitude of established AIH. Possible sex differences were also evaluated.

Results

NOXA1 expression in renal tubular epithelium is regulated by Ang II

Ang II is a potent inducer of *Nox1* expression in renal cells (9). We previously showed that Ang II induces NOXA1 expression in VSMCs (41). Because NOXA1 is required for NOX1 activation, we performed Western blot analysis of renal protein lysates from male wild-type mice treated with Ang II to test whether RAAS regulates NOXA1 expression in the kidney. NOXA1 expression increased significantly in the kidney 1 day after Ang II administration, with a sustained increase at 14 days (3.4- and 4.5-folds, respectively; Fig. 1A and Supplementary Fig. S5 A, B).

We next isolated suspensions of mouse proximal convoluted tubules (PCTs), thick ascending limb (TAL) of Henle, and CD. Western blot analysis showed NOXA1 expression in all nephron segments, with the highest expression in the CD (Fig. 1B and Supplementary Fig. S5 C, D). Immunofluorescence analysis of kidney coronal sections from the wild-type mice showed robust expression of NOX1 and NOXA1 in tubular epithelial cells (Fig. 1C, D). Specifically, expression of immunoreactive NOX1 and NOXA1 colocalized with aquaporin 1 (AQP1) expression in PCT, Na-K-Cl cotransporter 2 (NKCC2) expression in TAL, and with aquaporin 2 (AQP2) expression in CD.

The NOX1 and NOXA1 expression was the highest in the AQP2-positive CD principal cells ($p < 0.001$ for NOX1; Fig. 1C and $p < 0.05$ for NOXA1; Fig. 1D). Importantly, expression of immunoreactive neutrophil cytosolic factor 2 (NCF2; p67phox, the NOXA1 functional homolog) and NOX2 was not observed in the AQP2-positive epithelial cells (Supplementary Fig. S1). These results demonstrate that NOXA1, along with NOX1, is expressed in renal tubular epithelium and CD principal cells, and is upregulated by chronic systemic Ang II administration.

Renal ROS levels correlate with NOXA1 expression

There are marked differences between male and female mice in the regulation of basal BP and AIH (60). To determine whether renal effects of Ang II in males *versus* females are regulated by NOXA1, we first measured *Noxa1* mRNA levels in kidneys from mice treated with vehicle or Ang II for 14 days. Treatment with Ang II significantly increased *Noxa1* expression in the male but not female mice ($p < 0.01$; Fig. 2A).

Ang II administration in male wild-type mice stimulated NOXA1 protein expression by threefold in the AQP2-positive CD epithelial cells (Fig. 2B). Basal NOXA1 levels were slightly lower, and Ang II had less pronounced effect on the protein levels in CD cells of female wild-type mice (1.5-fold; Fig. 2B). Expression of *Nox1* mRNA was also significantly upregulated by Ang II treatment in male wild-type but not *Noxa1*$^{-/-}$ mice or wild-type female mice ($p < 0.01$; Fig. 2C). Immunoreactive NOX1 expression colocalized with AQP2 was significantly lower in kidneys of control- and Ang II-treated male *Noxa1*$^{-/-}$ and female wild-type compared with the respective male wild-type mice (Fig. 2D).

Similarly, Western blot analysis of whole kidney lysates showed a 1.5-fold increase in NOX1 protein levels in male mice after Ang II treatment but remained unchanged in female or *Noxa1*$^{-/-}$ mice (Fig. 2E and Supplementary Fig. S6A). NOX4 protein expression in whole kidney lysates was similar in wild-type and *Noxa1*$^{-/-}$ mice, and was equally upregulated by 14-day Ang II treatment in both genotypes. In contrast, immunoreactive NOX4 expression did not change in AQP2-positive CD cells with Ang II treatment, and was not different between wild-type and *Noxa1*$^{-/-}$ kidneys (Supplementary Fig. S2 and Supplementary Fig. S6B).

Increased NOXA1 expression is associated with increased NOX1 activity and ROS generation in the vasculature (41). Accordingly, $O_2^{\bullet-}$ levels determined by dihydroethidium (DHE) fluorescence were significantly increased in the kidneys

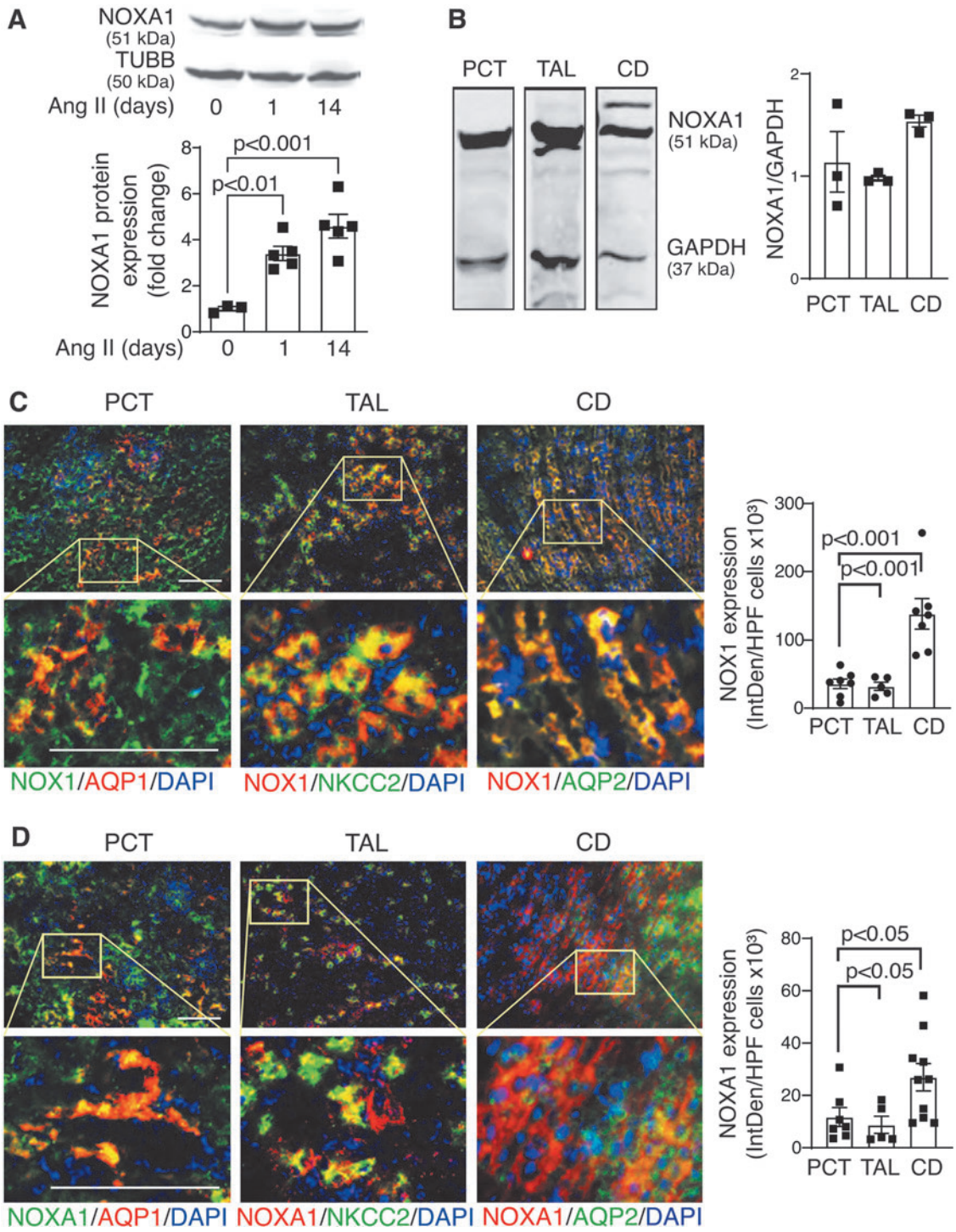

FIG. 1. NOXA1 protein expression in kidney is regulated by Ang II. (A) Western blot analysis and quantification of NOXA1 expression in kidney lysates after 1 and 14 days of Ang II treatment. Data are NOXA1 protein fold change relative to untreated control adjusted for β-tubulin levels (mean ± SEM). **(B)** Western blot analysis and relative expression quantification of protein extracts from isolated PCT, TAL, and CD. **(C)** Representative immunofluorescence images and quantification of immunoreactive NOX1 and AQP1 (colocalized to PCT), NKCC2 (colocalized to TAL), or AQP2 (colocalized to CD) in wild-type kidney frozen sections (mean ± SEM). High magnification *insets* (*yellow rectangle*) show NOX1 expression in epithelial cell. Scale is 100 μm. **(D)** Representative immunofluorescence images and quantification stained for immunoreactive NOXA1 and AQP1 (colocalized to PCT), NKCC2 (colocalized to TAL), or AQP2 (colocalized to CD) in wild-type kidney frozen sections (mean ± SEM). High magnification *insets* (*yellow rectangle*) show NOXA1 expression in epithelial cell. Scale is 100 μm. Ang II, angiotensin II; AQP1, aquaporin 1; CD, collecting ducts; NKCC2, Na-K-Cl cotransporter 2; NOX, NADPH oxidase; NOXA1, NOX activator 1; PCT, proximal convoluted tubules; TAL, thick ascending limb.

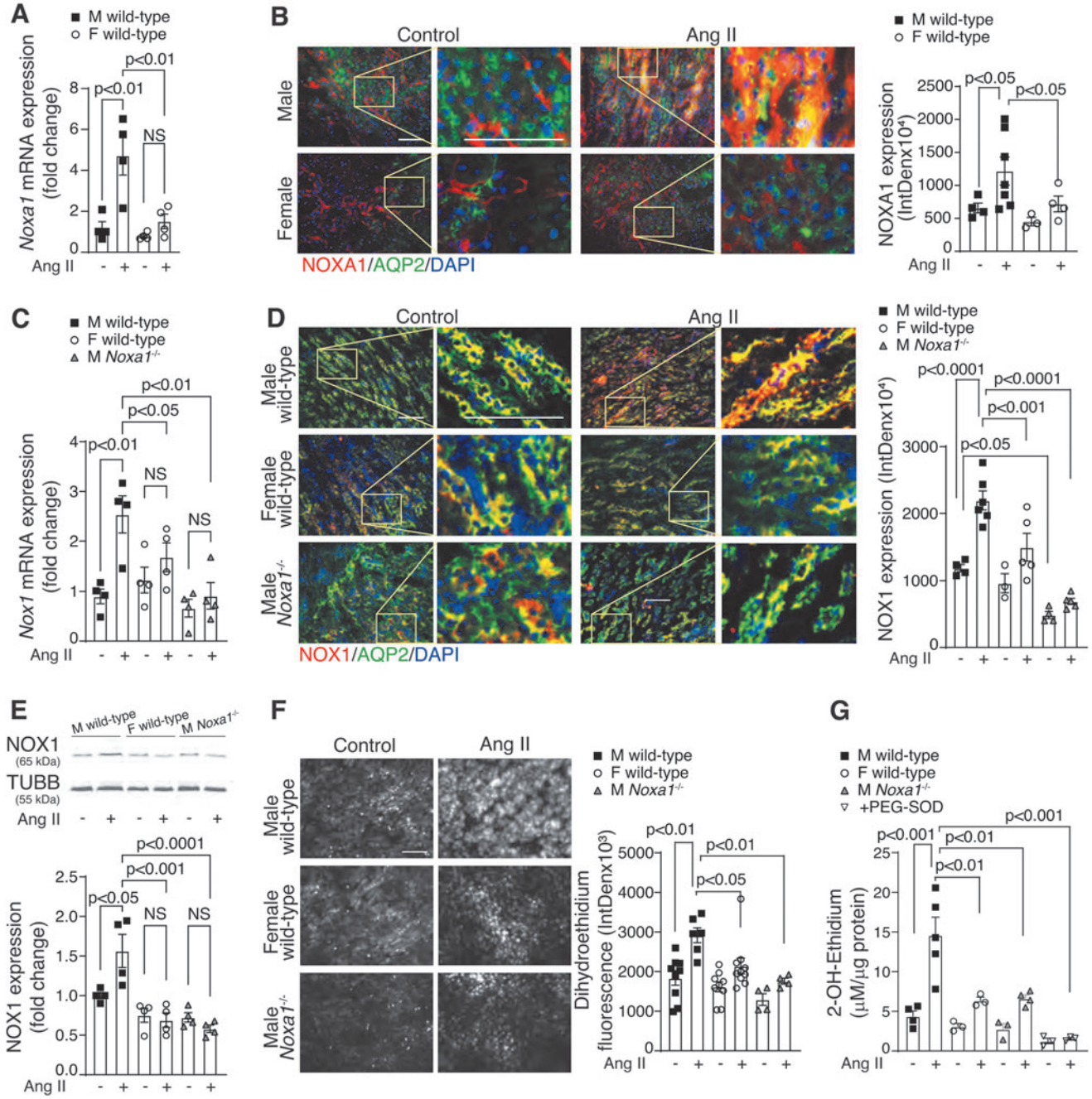

FIG. 2. NOXA1 expression is correlated with renal ROS levels in kidneys from wild-type mice treated with Ang II. **(A)** Real-time PCR analysis of *Noxa1* mRNA expression in kidneys from male (M) and female (F) mice treated with vehicle or Ang II for 14 days. Data are mean ± SEM of mRNA expression fold change relative to vehicle-treated control adjusted for 18s RNA levels. **(B)** Representative immunofluorescence images and quantification of NOXA1 (*red*) levels in the AQP2-stained CD epithelial cells (*green*) in the kidney sections of male and female mice treated with vehicle or Ang II for 14 days. High magnification *insets* (*yellow rectangle*) show NOXA1 expression in CD epithelial cell. Scale is 100 μm. Data are fluorescence integrated density (mean ± SEM). **(C)** Real-time PCR analysis of *Nox1* mRNA expression in kidneys from male wild-type and *Noxa1*$^{-/-}$ and female wild-type mice treated with vehicle or Ang II for 14 days. Data are mean ± SEM of mRNA expression fold change relative to vehicle-treated control adjusted for 18s RNA levels. **(D)** Representative immunofluorescence images and quantification of NOX1 (*red*) levels in the AQP2-positive CD epithelial cells (*green*) in the kidney sections of male and female wild-type and male *Noxa1*$^{-/-}$ mice treated with vehicle or Ang II for 14 days. High magnification *insets* (*yellow rectangle*) show NOX1 expression in CD epithelial cell. Scale is 100 μm. Data are fluorescence integrated density (mean ± SEM). **(E)** Western blot analysis and quantification of NOX1 protein expression in whole kidney lysates from mice treated with vehicle or Ang II for 14 days. Data are mean ± SEM of protein levels fold change relative to vehicle-treated control adjusted for TUBB levels. **(F)** ROS levels were determined by DHE fluorescence in the coronal renal sections of male and female wild-type and male *Noxa1*$^{-/-}$ mice treated with vehicle or Ang II for 14 days. Data are DHE fluorescence integrated density (mean ± SEM). **(G)** Superoxide levels in kidney samples from mice treated with vehicle or Ang II for 14 days were determined by 2-OH-ethidium HPLC. Data were normalized to tissue protein concentration (mean ± SEM). DHE, dihydroethidium; PCR, polymerase chain reaction; ROS, reactive oxygen species; TUBB, β-tubulin.

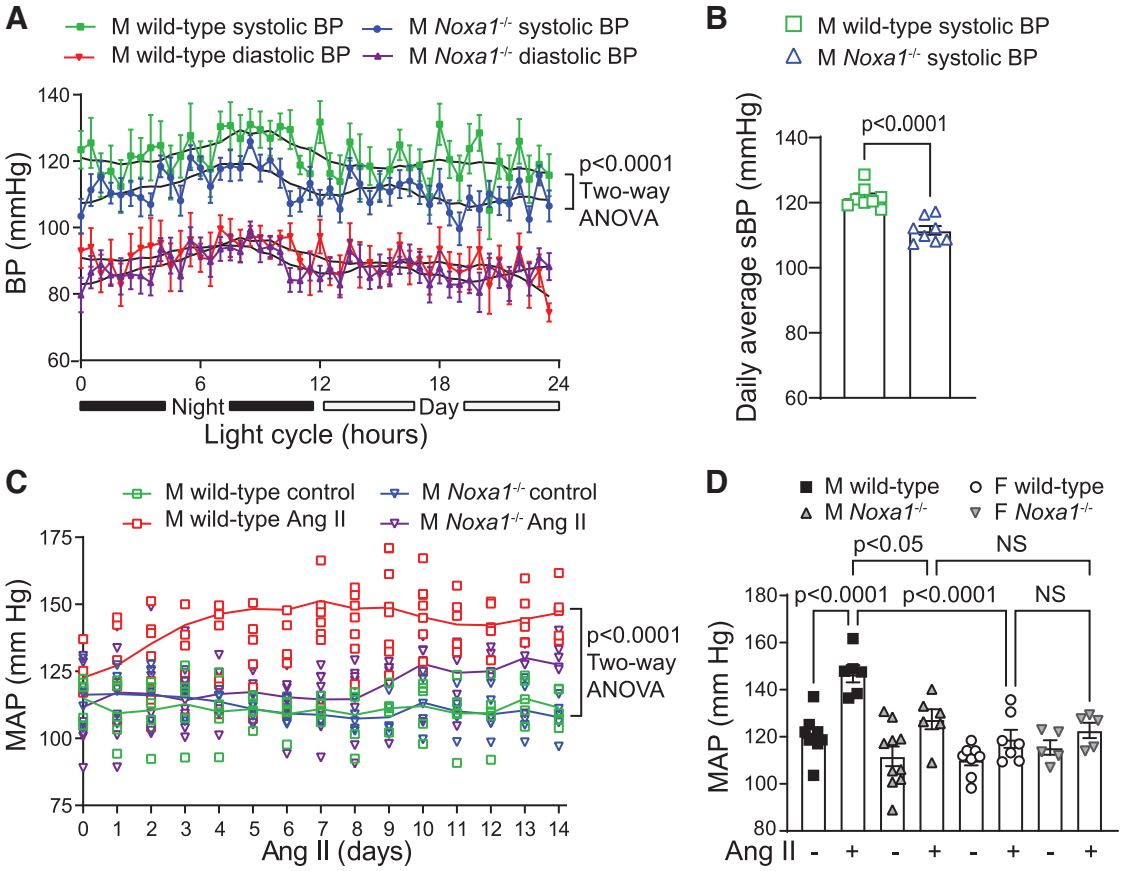

FIG. 3. ***Noxa1*** **deletion reduces basal and Ang II-induced BP in male mice. (A)** BP telemetry recordings averaged for 5 min every 30 min over 24-h period in untreated male (M) wild-type and *Noxa1*$^{-/-}$ mice (mean ± SEM, $n = 8$). Individual values for each animal are shown in Supplementary Figure S3. *Black solid lines* represent averages of 7 nearest neighbor values using second-order smoothing polynomial. **(B)** Daily average of sBP telemetry recordings in untreated male wild-type and *Noxa1*$^{-/-}$ mice (mean ± SEM). **(C)** Mean BP telemetry recordings in male wild-type and *Noxa1*$^{-/-}$ mice treated with vehicle or Ang II for 14 days. Data are mean ± SEM of daily average BP. **(D)** Mean BP telemetry recordings in male (M) and female (F) wild-type and *Noxa1*$^{-/-}$ mice treated with vehicle or Ang II for 14 days. Data are mean ± SEM of daily average BP. BP, blood pressure; sBP, systolic BP.

of male mice during Ang II treatment (Fig. 2F). ROS levels mirrored the sex differences in NOXA1 expression, with weaker induction by Ang II at 14 days in the epithelial cells of female wild-type mice kidneys. Similarly, *Noxa1*$^{-/-}$ male mice had significantly lower ROS levels in the kidney after Ang II administration compared with the wild-type mice.

Measurement of superoxide generation in kidney samples using 2-hydroxyethidium HPLC analysis also similarly showed significant reduction of superoxide in kidneys of female wild-type and male *Noxa1*$^{-/-}$ mice treated with Ang II compared with male wild-type mice (Fig. 2G). These results indicate that higher Ang II-induced ROS levels in male kidneys at least partially depend on the renal NOXA1 expression, while decreased renal ROS levels in female mice correlate with lower NOXA1/NOX1 expression and NOX1 activity.

Noxa1 *deletion attenuates AIH*

Because NOX1 was previously implicated in the regulation of BP (16) and NOXA1 regulates NOX1 activity, we performed continuous BP telemetry in conscious unrestrained male wild-type and *Noxa1*$^{-/-}$ mice. Analysis of 24-h BP recording showed a normal diurnal pattern in both genotypes (Fig. 3A). There was no difference in diastolic pressure; however, systolic BP was significantly lower in *Noxa1*$^{-/-}$ compared with the wild-type mice ($p < 0.0001$; two-way analysis of variance [ANOVA]).

The daily average systolic pressure was significantly lower in *Noxa1*$^{-/-}$ compared with wild-type mice (113 and 121 mmHg, respectively: Fig. 3B). Chronic Ang II administration induced a progressive increase in BP in wild-type as early as 1 day and reached a plateau ~5–7 days (+30 mmHg, $p < 0.0001$, two-way ANOVA; Fig. 3C). In contrast, chronic Ang II produced a less pronounced increase in the mean BP (+7 mmHg) in male *Noxa1*$^{-/-}$ mice (Fig. 3C).

AIH is attenuated in female mice

To test whether lower NOXA1 levels in female mice affect BP levels in AIH, we analyzed BP telemetry data in female mice during chronic Ang II administration. The response of female wild-type mice to Ang II was similar to *Noxa1*$^{-/-}$ male mice. Mean BP in wild-type females was stable with a small change at 14 days of Ang II infusion (+8 mmHg, Fig. 3D), similar to that observed in control female mice receiving infusion of isotonic saline.

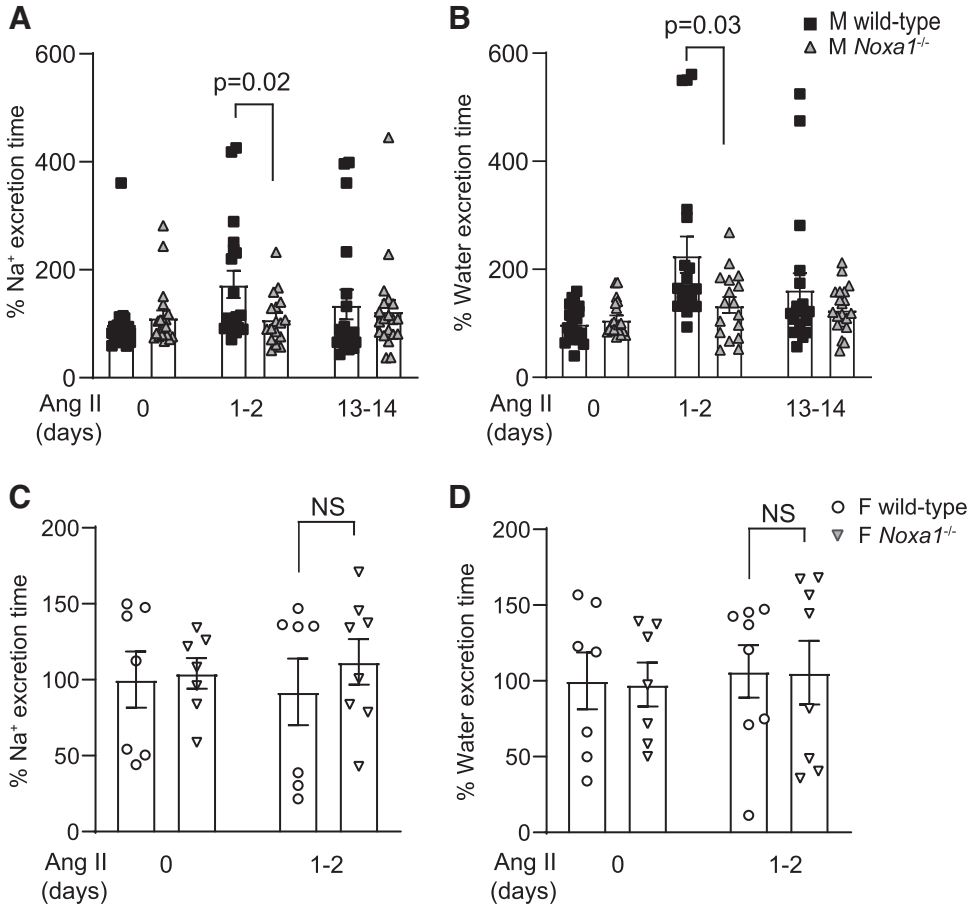

FIG. 4. Cumulative sodium and volume excretion is delayed in male wild-type mice compared with *Noxa1*$^{-/-}$ male and female wild-type mice during the initial phase of AIH. Time to excrete 75% of the sodium **(A)** and water **(B)** following the acute isotonic saline load in male wild-type and *Noxa1*$^{-/-}$ mice during the control period and Ang II infusion days 1–2 and 13–14. Data are mean ± SEM % over control. Time to excrete 75% of the sodium **(C)** and water **(D)** following the acute salt load in female wild-type and *Noxa1*$^{-/-}$ mice during the control period and Ang II administration for 1–2 days. Data are mean ± SEM % over control. AIH, Ang II-induced hypertension.

The response of female *Noxa1*$^{-/-}$ mice to Ang II was similar to that in female wild-type and male *Noxa1*$^{-/-}$ mice (+7 mmHg, Fig. 3D). Two-way ANOVA showed significant interaction between treatment and sex on BP ($p < 0.0001$). Thus, chronic sustained Ang II infusion produces HTN, and genetic deletion of *Noxa1* protects against the development of AIH in male mice, consistent with a more potent stimulation of NOXA1 expression and ROS production in the kidneys of wild-type males *versus* female mice.

Noxa1 deficiency preserves natriuresis in early phase of AIH

To evaluate the possible contribution of renal salt retention to the development of AIH, we analyzed renal excretion of Na^+ (urinary Na^+ excretion [UNaV]) and water over a 6–8-h period in response to acute saline load in conscious, unrestrained mice before and during AIH. During control conditions (before Ang II infusion), both male wild-type and *Noxa1*$^{-/-}$ mice excreted ~80%–90% of administered Na^+ and fluid over the 8-h collection period.

An important observation was that wild-type male mice exhibited less efficient renal excretion in response to an acute load of isotonic saline early during Ang II administration as evidenced by a markedly delayed Na^+ and water excretion compared with *Noxa1*$^{-/-}$ mice. Wild-type animals required a significantly greater time to excrete 75% of the Na^+ and volume challenge on days 1–2 of Ang II compared with *Noxa1*$^{-/-}$ mice (Na^+ excretion: 173% *vs.* 109% over control, $p = 0.02$; water excretion: 226% *vs.* 134% over control, $p = 0.03$; Fig. 4A, B).

Thus, this period of relative renal Na^+ and water retention was associated with an early phase of HTN development when BP began to rise rapidly, indicating a primary causative defect in renal tubular reabsorption, which was alleviated by *Noxa1* deletion. The rate of renal excretion of Na^+ and water was similar in both groups after days 13–14 of Ang II infusion. The normalization of Na^+ and water excretion by the elevated BP in male wild-type mice during sustained AIH implicates pressure–natriuresis in offsetting the early phase of Na^+ retention.

Because female mice showed attenuated NOXA1-dependent ROS generation and BP increase induced by Ang II, we also evaluated their ability to excrete Na^+ and water in response to an acute challenge. The time to excrete 75% of Na^+ and water loads during days 1–2 of Ang II administration did not differ between female wild-type and *Noxa1*$^{-/-}$ mice, and were similar to control wild-type male mice (Fig. 4C, D). These data confirm the notion that NOXA1 expression and activity are critical for RAAS-regulated natriuresis, and that sex differences in renal epithelium NOXA1 levels may have a causal role in the magnitude of AIH.

NOXA1 is required for RAAS-dependent regulation of renal ENaC

RAAS-dependent regulation of Na^+ transporting proteins is a major regulatory mechanism of Na^+ excretion and tubular

reabsorption (25). We evaluated the levels of Na^+ transport proteins present in the sites with predominant NOXA1 expression in the kidney from mice treated with Ang II for 14 days. The Western blot analysis of renal lysates showed no significant differences in expression of NKCC2 (expressed in the TAL), Na-H exchanger 3 (NHE3 in the PCT), or Na-Cl cotransporter (NCC in the distal convoluted tubules) between the wild-type and *Noxa1*$^{-/-}$ mice (Fig. 5A and Supplementary Fig. S7 A–D).

In contrast, the expression of αENaC was significantly induced by Ang II treatment in wild-type but not in *Noxa1*$^{-/-}$ mouse kidneys ($p < 0.0001$; Fig. 5B and Supplementary Fig. S7 E, F). Furthermore, immunofluorescence analysis of kidney coronal sections showed a significant increase of αENaC levels in CD principal cells costained with AQP2 1 day after Ang II administration in the wild-type but not in *Noxa1*$^{-/-}$ mice (Fig. 5C, $p < 0.01$). The αENaC level in wild-type kidneys declined by day 14 of Ang II treatment but was still significantly higher compared with control wild-type mice or Ang II-treated *Noxa1*$^{-/-}$ mice.

Aldosterone-dependent activity of ENaC is regulated by increased transcription (46) as well as by ENaC translocation to the apical plasma membrane (15). The ENaC immunofluorescence was localized closer to basolateral membrane of CD cells in vehicle-treated kidneys, but increased in intensity and extended toward the apical membrane in the wild-type ($p < 0.01$; Fig. 5D) but not in *Noxa1*$^{-/-}$ mice treated with Ang II for 1 day.

These results suggest that increased NOXA1-dependent ROS generation in the kidney during AIH promotes Na^+ retention in part through upregulation of ENaC expression in CD cells. The peak expression level and localization of ENaC to apical membrane of CD cells correlated with reduced UNaV in the wild-type mice. Both the processes were unaffected in the *Noxa1*$^{-/-}$ mice.

To better understand the cellular mechanisms of RAAS-dependent ENaC regulation, we assessed NOX expression and activity in M1 mouse CD cells treated with aldosterone, the mineralocorticoid hormone induced by Ang II treatment (27, 47). M1 cells expressed *Noxa1*, *Nox1*, *Ncf1/2,* and *Nox4* genes, and treatment with aldosterone significantly increased the expression of *Noxa1* but not the other NOX subunit genes (Fig. 6A). Aldosterone treatment significantly increased superoxide levels in M1 cells, and pretreatment with diphenyliodinium, an inhibitor of NOX, significantly reduced aldosterone-induced superoxide generation (Fig. 6B).

In contrast, oxypurinol, an inhibitor of xanthine oxidase, L-Nitro arginine methyl ester, an inhibitor of nitric oxide synthase, and N-acetyl cysteine, a glutathione precursor, did not have a significant effect on aldosterone-induced ROS generation, suggesting that NOX is a primary source of superoxide in renal epithelial cells. To study the effects of NOXA1 expression on NOX1 activity in M1 cells, we used *Noxa1* small-interfering RNA (siRNA):p5RHH peptide nanocomplexes (30, 53).

Cells transduced with *Noxa1* siRNA showed selective and significant reduction (>50%) of *Noxa1* mRNA and protein without changes in *Nox1* or *Ncf1/2* gene expression (Supplementary Fig. S4A, B and Supplementary Fig. S8A). Aldosterone treatment significantly increased superoxide generation in M1 cells, and pretreatment with polyethylene glycol-conjugated superoxide dismutase (PEG-SOD) attenuated this response ($p < 0.0001$; Fig. 6C). Furthermore, aldosterone-induced superoxide generation was significantly lower in the cells transduced with *Noxa1* siRNA ($p < 0.0001$ *vs.* control cells) but not with scrambled siRNA.

Similarly, M1 cells transduced with *Nox1* siRNA had significantly reduced *Nox1* mRNA and protein (>50%) levels (Fig. 6D and Supplementary Fig. S4C and Supplementary Fig. S8B), and aldosterone treatment had no significant effect on ROS generation in *Nox1* siRNA-transduced cells as compared with control or scrambled siRNA-transduced cells ($p < 0.0001$; Fig. 6C).

Congruently, real-time polymerase chain reaction (PCR) analysis demonstrated that transduction of M1 cells with *Noxa1* siRNA, but not scrambled siRNA, markedly reduced *Noxa1* levels in the control cells and abrogated aldosterone-induced increase in *Noxa1* mRNA expression (Fig. 6E). These results demonstrate that NOX is a primary source of superoxide in renal epithelial cells, and that aldosterone-induced NOX activation and superoxide generation are dependent on NOXA1 expression.

Aldosterone treatment significantly increased *Scnn1a* (αENaC) mRNA levels in control and scrambled siRNA-transduced but not in *Noxa1* or *Nox1* siRNA-transduced M1 cells, indicating that aldosterone-induced ENaC expression in the renal epithelial cells is dependent on the initial activation of NOXA1/NOX1 NADPH oxidase (Fig. 6F).

Furthermore, congruent with siRNA transduction, pretreatment of M1 cells with PEG-SOD abrogated aldosterone-induced *Scnn1a* upregulation, implying that NOXA1/NOX1 NADPH oxidase is the major source of superoxide and regulates expression of ENaC in renal epithelial cells. Similar to kidney CD cells, confocal microscopy analysis of polarized M1 cell monolayer demonstrated that aldosterone markedly induced ENaC expression and translocation to the apical membrane as shown by colocalization with the tight-junction protein occludin (Fig. 6G).

FIG. 5. Renal expression of ENaC is increased in male wild-type mice treated with Ang II. (A) Western blot analysis and densitometry quantification of the sodium channels NHE3, NKCC2, and NCC expression in mice treated with Ang II for 14 days. Data are fold change in protein expression adjusted for ACTB levels and relative to wild-type (mean ± SEM). **(B)** Western blot analysis and densitometry quantification of βENaC levels in renal lysates from wild-type and *Noxa1*$^{-/-}$ mice treated with vehicle or Ang II for 14 days. Data are protein fold change adjusted for ACTB levels and relative to control (mean ± SEM). **(C)** Representative immunofluorescence images and quantification of αENaC expression in the renal sections from wild-type and *Noxa1*$^{-/-}$ mice treated with vehicle or Ang II for 1 or 14 days, and stained for αENaC (*red*), AQP2 (*green*), and DAPI (*blue*). High magnification *insets* (*yellow rectangle*) show αENaC expression in CD epithelial cell. Scale is 100 μm. Data are fluorescence integrated density (mean ± SEM). **(D)** Representative immunofluorescence images and quantification of αENaC colocalization with AQP2 on the apical (A) or basolateral (BL) side of the CD cells from wild-type and *Noxa1*$^{-/-}$ mice treated with vehicle or Ang II for 1 day, and stained for αENaC (*red*), AQP2 (*green*), and DAPI (*blue*). Data are fluorescence integrated density (mean ± SEM). Scale is 10 μm. ACTB, β-actin; ENaC, epithelial Na^+ channel; NCC, Na-Cl cotransporter; NHE3, Na-H exchanger 3.

Fluorescence densitometry showed that, consistent with NOXA1-dependent ENaC activation, apical membrane localization of ENaC was markedly reduced in *Noxa1* siRNA but not scrambled siRNA-transduced M1 cells treated with aldosterone. Taken together, these data affirm the critical role of NOXA1 in RAAS-dependent activation of ROS-induced ENaC activity and Na^+ transport in renal epithelial cells to promote renal Na^+ and water retention and BP regulation in the developmental stage of AIH.

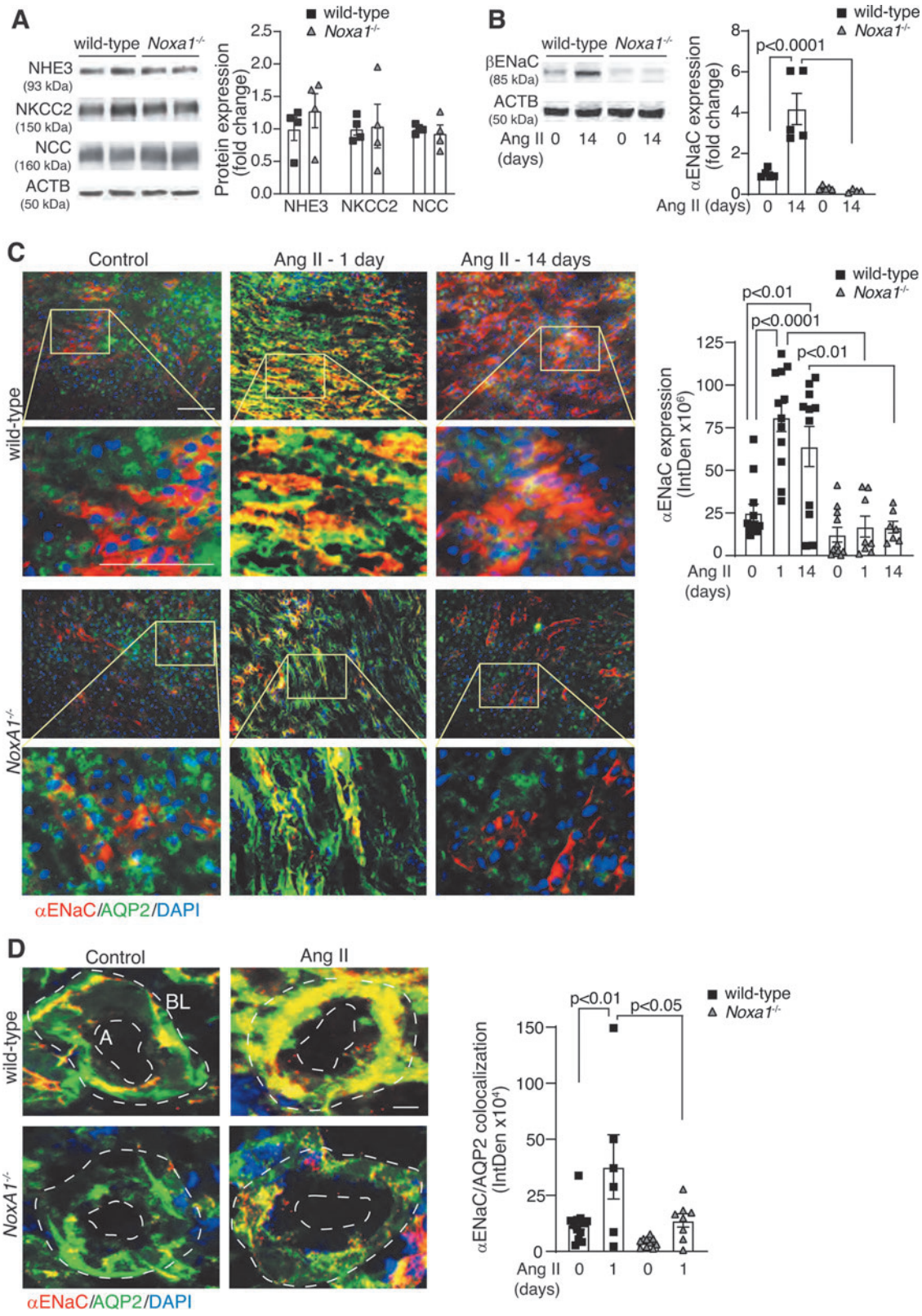

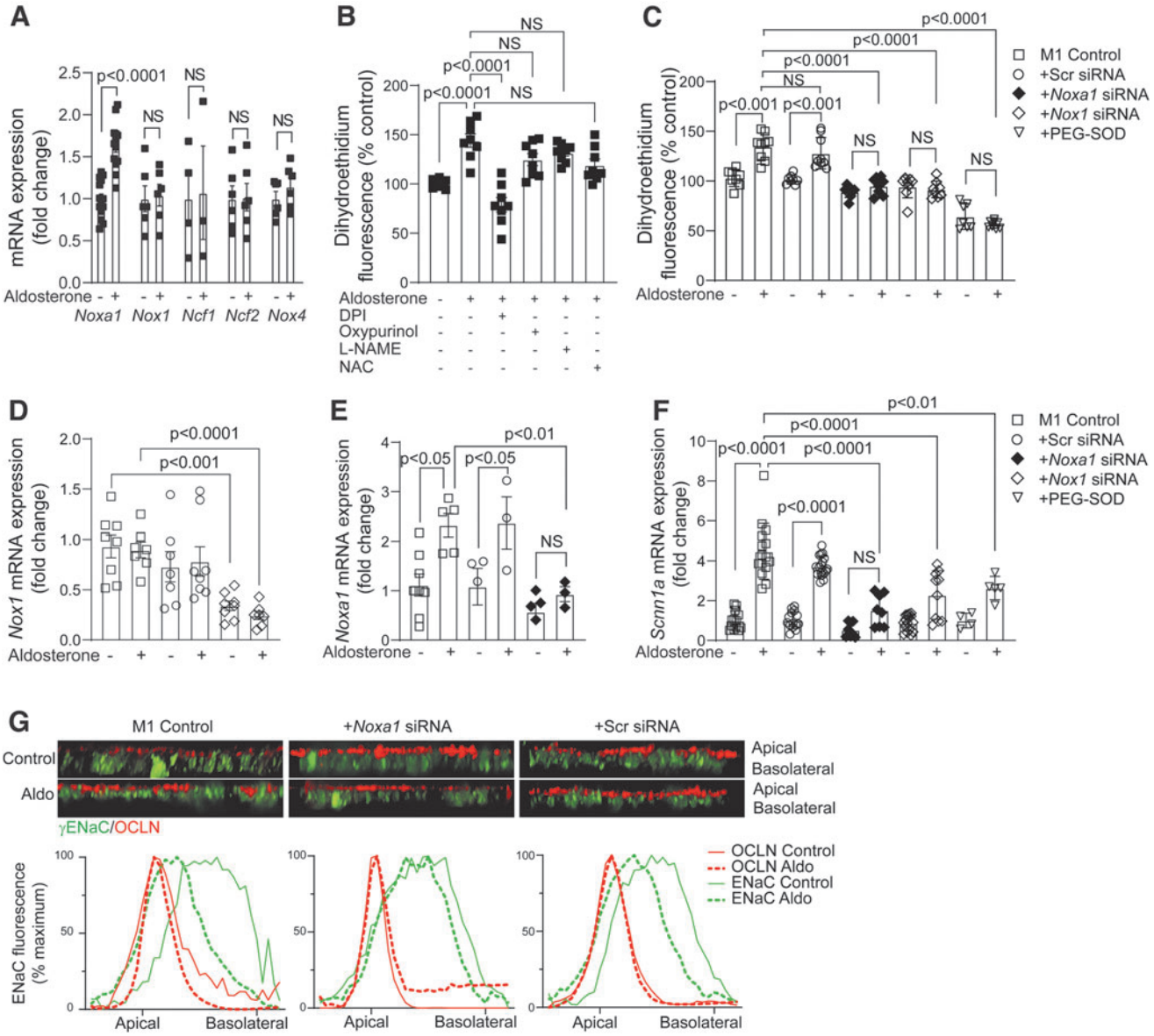

FIG. 6. ENaC is regulated through aldosterone activation of NOXA1-dependent NOX in M1 renal epithelial cells. **(A)** Real-time PCR analysis of *Nox1*, *Noxa1*, *Ncf1/2* (p47phox/p67phox), and *Nox4* expression levels in M1 renal epithelial cells treated with vehicle or aldosterone for 2 h. Data are mean ± SEM of mRNA expression adjusted to 18s RNA levels. **(B)** DHE fluorescence was measured in M1 cells treated with vehicle or aldosterone for 30 min, or cells pretreated with 10 μM DPI, 50 μM oxypurinol, 10 μM L-NAME, or 20 mM NAC and then treated with aldosterone. Data are mean ± SEM of DHE fluorescence as percentage of control vehicle-treated cells. **(C)** DHE fluorescence was determined in control- or PEG-SOD treated M1 cells, or cells transduced with *Noxa1*, *Nox1,* or scrambled siRNA, and then treated with vehicle or aldosterone for 30 min. Data are mean ± SEM of DHE fluorescence as percentage of control-untreated cells. **(D)** Real-time PCR analysis of *Nox1* mRNA expression in control and scrambled siRNA or *Nox1* siRNA-transduced cells treated with aldosterone for 2 h. Data are mean ± SEM of mRNA expression fold change relative to control adjusted for 18s RNA levels. **(E)** Real-time PCR analysis of *Noxa1* mRNA expression in control and scrambled siRNA or *Noxa1* siRNA-transduced cells treated with aldosterone for 2 h. Data are mean ± SEM of mRNA expression fold change relative to control adjusted to 18s RNA. **(F)** Real-time PCR analysis of *Scnn1a* (αENaC) gene expression in control, PEG-SOD treated cells, or cells transduced with *Noxa1*, *Nox1,* or scrambled siRNA and treated with aldosterone for 2 h. Data are mean ± SEM of mRNA expression adjusted to 18s RNA. **(G)** Representative confocal microscopy z-stack images of polarized M1 renal epithelial cells treated with vehicle or aldosterone for 30 min, and stained for γENaC (*green*) and OCLN (*red*). Fluorescence quantification of apical and basolateral localization of γENaC in control and *Noxa1* siRNA- or scrambled siRNA-transduced M1 cells treated with vehicle or aldosterone. DPI, diphenyliodinium; NAC, N-acetyl cysteine; L-NAME, L-nitro arginine methyl ester OCLN, occluding; PEG-SOD, polyethylene glycol-conjugated superoxide dismutase; siRNA, small-interfering RNA.

Discussion

This study demonstrates that NOXA1 is a critical activator of NOX1 NADPH oxidase and ROS generation in renal epithelial cells in response to Ang II/aldosterone; NOXA1-dependent ROS generation regulates ENaC expression and activation in renal CD cells; increased expression of NOXA1 in renal epithelial cells in response to Ang II results in greater Na^+ and water retention, and ultimately increased BP in the developmental stage of HTN; *Noxa1* genetic deletion or targeting with siRNA decreases ROS levels, preserves natriuresis, and attenuates AIH. We also showed that less pronounced NOXA1/NOX1 activation in CD cells may provide relative protection against AIH in premenopausal females.

Our results are in line with the reports that genetic ablation of *Nox* genes or inhibition of ROS generation by NOX1 attenuates HTN (16, 35, 58). However, previous studies attributed the prohypertensive effects of RAAS to NOX1 activation primarily in the vasculature (13, 59). We present new evidence that Ang II acts to increase NOX1 mRNA and NOX1-dependent ROS production in the kidney. While chronic Ang II stimulation of other NOX isoforms in vascular (8, 13, 59), renal macula densa cells (65), and immune cells (5) was reported to contribute to HTN, we show, for the first time, that RAAS activation of NOXA1-dependent NOX1 in the CD regulates redox signaling and epithelial cell function, which are likely critical in early phases of salt retention and the development of HTN.

We observed that male wild-type mice with increased NOXA1-NOX1 signaling excrete acute Na^+ and water loads in a delayed manner during the first two days of Ang II infusion when BP begins to rise. Our results are supported by previous studies that reported sluggish UNaV at early stages of AIH in the wild-type mice (18, 33, 52), and in consonance with the published reports that renal retention of salt and water is a hallmark initiating event during the development of AIH.

The Ang II-induced NOXA1/NOX1/ROS signaling upregulating ENaC expression/activity we observed is consistent with the hypothesis that enhanced ENaC-mediated Na^+ reabsorption in the CD is responsible for an early phase of Na^+ retention in the wild-type males, contributing importantly to the development of many forms of HTN. We provide additional new information that genetic deletion of *Noxa1* leads to attenuated levels of $O_2^{\bullet-}$ and ENaC in the renal CD principal cells in response to Ang II. Thus, changes in ENaC expression are negatively associated with the efficiency of excreting an acute salt load, and higher ENaC levels are associated with delayed Na^+ excretion early during the development of AIH. These data support the notion that NOXA1 acts as a critical limiting factor in NOX1 activation in regulating Na^+ retention in AIH.

Patch-clamp studies of isolated CD showed Ang II-dependent stimulation of ENaC activity (32, 33, 43). Aldosterone is also a potent upregulator of αENaC expression in the CD cells (46) and increases its activity by promoting γENaC translocation to the apical membrane (15, 34). However, Ang II-dependent ENaC activation and Na^+ reabsorption in the mouse distal nephron might also be independent of aldosterone (32, 33). Ang II may activate ENaC in CD principal cells by increasing NOX-derived $O_2^{\bullet-}$ production through activation of protein kinase C (PKC) independent of intracellular Ca^{2+} levels (48). Importantly, NFκB may directly regulate αENaC transcription in renal epithelial cells (11).

This suggests a possibility of transcriptional induction of ENaC by NOX activation, without RAAS hyperactivation, under pathophysiological conditions such as hyperglycemia and increased systemic oxidative stress of CKD. Ang II stimulates NOX1 (13, 59) and consequently activates PKCδ (38, 40, 63). This, in turn, increases the abundance of the γENaC in the apical plasma membrane of CD cells (63), and PKCδ mediates aldosterone-induced *Nox1* gene expression (63), suggesting a feed-forward loop involving PKCδ and NOX1 in apical localization of γENaC by Ang II.

Moreover, increased NOXA1/NOX1-dependent $O_2^{\bullet-}$ levels might counteract nitric oxide inhibition of epithelial ENaC activity, increasing Na^+ reabsorption and BP in AIH (57, 62). Our results indicate that NOXA1-dependent ROS generation causes increased ENaC mRNA and protein expression and membrane assembly in CD epithelial cells and cultured M1 cells. In addition, we show that in M1 cells pretreated with PEG-SOD aldosterone-induced upregulation of ENaC was significantly attenuated, suggesting a critical role for superoxide in the regulation of ENaC transcription.

As we note, the initial phase of Na^+ retention during the development of AIH coincided with sustained upregulation of ENaC expression/activity in CD cells. However, there is a temporal disparity between ENaC expression/activity during established AIH when renal Na^+ excretion is normal. The prohypertensive transient early phase of enhanced renal retention of salt and water is offset by compensatory pressure natriuresis that normalizes Na^+ excretion in the presence of more long-standing increased BP.

Increased expression of αENaC on day 14 of AIH implies that continued enhanced Na^+ reabsorption in the CD is offset by the influence of a pressure-induced natriuresis, resulting from inhibition of Na^+ reabsorption at an upstream nephron site. Reduced Na^+ reabsorption mediated by proximal tubular NHE3 is thought to be a major participant in pressure natriuresis during the established phase of AIH (62).

Male sex is independently associated with the development of treatment-resistant HTN in CKD patients (51). Our observation that chronic Ang II produces less pronounced HTN in female than male wild-type mice is consistent with a previous report (60). Females appear to be protected from HTN by higher levels of estrogen and NO, less severe endothelial dysfunction, and a higher ratio of AT_2/AT_1 receptors and Ang 1–7/Ang II combined with lower levels of vasoconstrictor and antinatriuretic ROS (3, 7, 21, 56).

A study utilizing renal crosstransplantation indicates that the kidneys play a critical role in contributing to sex differences in AIH, with male kidneys being prohypertensive and female kidneys affording protection (56). Male kidneys have greater gene expression of AT_1 receptor, AT_1/AT_2 receptor ratio, proximal tubular NHE3, and distal nephron α- and γ-subunits of ENaC (56). We provide new information that the attenuated AIH in females is related to weaker Ang II stimulation of renal NOXA1 and ROS and the reduced upregulation of CD cell ENaC relative to changes in males. Indeed, estrogen treatment was shown to attenuate Ang II-induced NOX2 and p67phox expression in endothelial cells (19). Estrogen can exert inhibitory effects on gene expression

through several epigenetic mechanisms, including methylation of CpG islands of the gene promoter (2).

Similar mechanism may be involved in lowering the expression of *Noxa1*/*Nox1* and *Scnn1* genes in renal epithelial cells in females. This notion is supported by the observation of decreased fractional distal reabsorption of Na^+ during the follicular phase in normotensive women (42). Such sex differences appear to be responsible for more efficient excretory responses to an acute salt and water challenge and thus less renal retention.

CKD is often associated with elevated BP and the development of treatment-resistant HTN. We demonstrate that RAAS drives NOXA1/NOX1-dependent ROS generation in renal epithelial cells, which is a critical mechanism regulating Na^+ excretion and BP. Chronic disease-associated activation of renal NOXA1/NOX1 may be a potential mechanism of enhanced Na^+ reabsorption and BP elevation without apparent hyperactivation of RAAS.

Such conditions may render the therapeutic agents aimed at RAAS inhibition (angiotensin-converting enzyme inhibitors, angiotensin receptor blockers, mineralocorticoid receptor antagonists) ineffective, resulting in treatment-resistant HTN. Currently, there are no NOX subunit-specific inhibitors available for clinical use. GKT137831 or setanaxib, a member of a recently designated novel drug class, naxibs, showed promising therapeutic potential in HTN-related conditions (20, 64). Therapeutic strategies that reduce NOXA1/NOX1 activation and ROS generation in renal epithelial cells and/or inhibit ENaC hyperactivation may be beneficial in the treatment of CKD, diabetes, and HTN.

Materials and Methods

Animals

All animal procedures were performed in compliance with protocols approved by the University of Michigan and the University of North Carolina Institutional Animal Care and Use Committee in accordance with NIH OLAW policies. Male wild-type (C57BL/6J) mice were purchased from Jackson Laboratory (Bar Harbor, ME). The *Noxa1*$^{-/-}$ mice were generated by removing the coding region of mouse *Noxa1* gene as described previously (54). Mice were bred in-house, and littermates from heterozygous breeding were used in the experiments. Mice were housed in ventilated cages at 22°C with 12-h light/dark cycle and free access to food and water.

Renal tubules isolation

Suspensions of renal PCT, medullary TAL, and distal tubule or CD were prepared using published methods (4, 10).

BP telemetry

Male and female wild-type and *Noxa1*$^{-/-}$ 4-month-old mice were randomly assigned to control or treatment groups. Mice were surgically implanted with systemic BP transmitters (PA-C10; DSI, St. Paul, MN) under inhaled 1% isoflurane/O_2 anesthesia through carotid artery cannulation. After establishing basal level BP and appropriate diurnal cycling, mice were implanted with subcutaneous micro-osmotic pumps (Alzet 1002; Durect, Cupertino, CA) to continuously deliver a slow pressor dose of Ang II (500 ng/kg/min) (24, 52) or vehicle (0.9% NaCl) for 14 days. BP (mean, systolic, and diastolic) and heart rate were recorded in conscious unrestrained mice continuously for 5 min every 30 min. Data were collected and analyzed with Ponemah v6 (DSI), and BP daily moving average calculated for each day.

Cell culture

M1 mouse CD epithelial cells were obtained from ATCC (CRL-2038). The cells were maintained in Dulbecco's modified Eagle's medium (DMEM) and Ham's F12 medium mixture (11330; Thermo Fisher, Waltham, MA) supplemented with antibiotic/antimycotic solution, 5 μM dexamethasone (D-085; Sigma), and 5% fetal bovine serum (FBS) in 5% CO_2 incubator at 37°C. The cells were plated on Corning Transwell inserts (3413; Sigma) and incubated until transepithelial electrical resistance was measured to be >1 kΩ with a EVOM2 meter (World Precision Instruments, Sarasota, FL) to allow for polarization of the cell layer.

The cells were growth arrested for 24 h in DMEM supplemented with 0.1% FBS, and then incubated with 10 μM aldosterone (Sigma) in FBS-free DMEM. Mouse ON-TARGET*plus* SMARTpool *Noxa1* siRNA (LQ-064237-02-0020), *Nox1* siRNA (L-054651-00-0005), and nontargeting pool siRNA (D-001810-10-20) were purchased from Dharmacon (Lafayette, CO). M1 cells were transfected using p5RHH peptide–siRNA nanocomplexes as described (30, 53). Quiescent cells were incubated with nanocomplexes for 4 h at 37°C, and then treated with aldosterone.

Histology, immunostaining, and confocal microscopy

Mice were euthanized with an overdose of inhaled isoflurane, the circulatory system was perfused with phosphate-buffered saline, and renal arteries and kidneys were dissected, embedded in O.C.T. compound (Sakura Finetek, Torrance, CA), and snap-frozen in liquid nitrogen. Coronal sections of 10 μm thickness were cut from dissected kidneys.

Frozen kidney sections were fixed in acetone, permeabilized in 0.1% Triton X-100, and immunofluorescent staining was performed using antibodies against NOXA1 (Ab199; a gift from Dr. Ralf Brandes, Institut für Kardiovaskuläre Physiologie, Goethe-Universität, Frankfurt am Main, Germany) (41), NOX1, NOX2, or NCF2 (bs-3682R, bs-3889R, bs-3891R; Bioss, Woburn, MA), ENaC-α (SPC-403D; StressMarq, Victoria, BC, Canada) followed by goat antirabbit secondary antibody conjugated to AlexaFluor 594 or Alexa Fluor 488 (A11072, A27034;Thermo Fisher) and Cy3-conjugated AQP1, AlexaFluor 488-conjugated AQP2 (bs-1506R-Cy3, bs-4611R-A488; Bioss), or FITC-conjugated NKCC2 antibody (SPC-401D-FITC; StressMarq).

Sections were mounted with Vectashield mounting medium for fluorescence with 4′,6-diamidino-2-phenylindole (H-1200; Vector Laboratories). Fluorescence images were acquired with Nikon Microphot-FX microscope using the same exposure, gain and offset values.

M1 cells plated on Transwell inserts and polarized before treatment were used for confocal microscopy. Z-stacks were acquired using a Nikon Eclipse Ti microscope using the same exposure, gain and offset values. M1 cells were fixed on the Transwell membrane with methanol at −20°C, washed with phosphate-buffered saline (PBS), permeabilized with 0.01% Triton X-100, and blocked with 3% bovine serum albumin

(BSA)/1% goat serum. Primary antibodies used were ENaC-γ (ab3468; Abcam, Cambridge, United Kingdom) and Alexa-Fluor 594-conjugated occludin antibody (OCLN, 331594; Invitrogen) for detection of the apical membrane (36).

Volume views of the orthogonal plane were created in NIS Elements software (Nikon). Positional information was analyzed by measuring the integrated density of each slice in the z-stack using NIH ImageJ 1.49 (Bethesda, MD). Plots of the relative amount of integrated density were made, and the position of both channels was adjusted so that OCLN staining overlapped when making comparisons.

ROS measurements

ROS levels were measured *in situ* as described before (53). Fresh frozen renal coronal sections were incubated with 10 μm DHE (Thermo Fisher) in the presence or absence of 200 U/mL PEG-SOD (Sigma) in Hank's balanced salt solution (HBSS) at 37°C for 15 min. Fluorescence images were acquired with Nikon Microphot-FX microscope using monochrome camera at the same exposure, gain and offset values. Images were analyzed using NIH ImageJ, and mean gray value per arterial wall area (integrated density) was determined.

Measurement of superoxide in renal tissues was performed using HPLC detection of 2-hydroxyethidium. Dissected kidney samples were minced and incubated with 50 μM DHE for 30 min. Control samples were incubated with 200 U/mL PEG-SOD (Sigma) prior incubation with DHE. The excess DHE was removed, and tissues were homogenized in acetonitrile. The supernatants were collected and dried using Savant ISS 100 (Thermo Scientific).

Samples were dissolved in PBS, and 50 μL were analyzed using Agilent 1100 HPLC system (Agilent Technologies, Santa Clara, CA) equipped with Partisil 5 μm ODS3 250 × 4.6 mm column (Phenomenex, Torrance CA). Chromatograms were analyzed with OpenLab software (Agilent Technologies). Superoxide levels were quantified using oxyethidium standard (Noxygen Science Transfer & Diagnostics GmbH, Elzach, Germany).

M1 cells were cultured in black clear-bottom 96-well plates and incubated with 10 μm DHE in the presence or absence of 200 U/mL PEG-SOD (Sigma) in HBSS. Fluorescence (518 nm excitation/606 nm emission) was determined after 1 h incubation using SpectraMax iD5 microplate reader (Molecular Devices). Measurements were analyzed with SoftMax Pro7 software (Molecular Devices).

Reverse transcription-polymerase chain reaction and Western blot analysis

Total RNA from homogenized renal tissue and M1 cells was isolated using RNeasy Micro Kit (74004; Qiagen, Hilden, Germany) according to manufacturer's protocol. Reverse transcription PCR for cDNA synthesis was performed using iScript Reverse Transcription Supermix (1708891; Biorad, Hercules, CA). Real-time PCR was performed on the 7900 HT Sequence Detection System using TaqMan PCR Master Mix (4304437; Applied Biosystems, Foster City, CA) and TaqMan Gene Expression Assays for 18s RNA (Mm03928990_g1), *Noxa1* (Mm00549175_m1), *Scnn1a* (Mm00803386_m1), *Nox1* (Mm00549170_m1), *Ncf1* (Mm00447921_m1), and *Ncf2* (Mm00726636_s1).

Total protein from mouse kidney was extracted using T-PER Mammalian Protein Extraction Reagent supplemented with Halt Protease Inhibitor Cocktail and EDTA (78510; ThermoFisher). After 30 min incubation on ice and centrifugation at 16,000 *g* for 10 min at 4°C, the supernatant was retained for protein analysis. Concentration of protein was determined using BCA protein assay (23227; Thermo Fisher). Equal amounts of protein lysates were resolved on 10% sodium dodecyl sulfate–polyacrylamide gels by electrophoresis and transferred into a nitrocellulose membrane (10600002; GE Healthcare, Chicago, IL).

After washing and blocking in Blocker™ BSA in TBS (37520; Thermo Fisher), membranes were incubated with a primary antibody, and then with a matching secondary fluorescently labeled antibody IRDye® 800CW (926-32210; Li-Cor, Lincoln, NE) or IRDye® 680CW (926-68071; Li-Cor). Primary antibodies used in these studies include NOXA1(Ab199), NOX1, NOX4 (ab131088, ab109225; Abcam), (NKCC2, NCC, ENaC-α (SPC-401D, SPC-402D, SPC-403D; Stressmarq), NHE3 (NHE31-A; Alpha Diagnostics, San Antonio, TX), GAPDH (2118; Cell Signaling), β-tubulin (T-0198; Sigma), and β-actin (A2228; Sigma). Detection of fluorescent signal was performed on imaging system Odyssey® CLx (Li-Cor). The intensity of the bands was analyzed using NIH ImageJ software.

Renal Na^+ and water excretion measurement

Urinary Na^+ and water excretion was assessed in conscious unrestrained mice as previously described (50, 52). In brief, mice housed individually in the metabolic cages (UNO, Zevenaar, Netherlands) were intraperitoneally injected with isotonic saline (0.9% NaCl, 37°C) equivalent of 10% body weight, and the urine was collected under oil every 2 h over 8 h (52). The AIH developmental phase was equated with Ang II infusion for 1 day and an established phase of HTN—after Ang II administration for 14 days. Urine volume was measured gravimetrically. Urine Na^+ concentration was measured by flame photometry (IL 943 Flame Photometer, Lexington, MA). UNaV was calculated as urine Na^+ concentration × urine flow rate.

Statistical analysis

All analyses were performed using Prism 8 (GraphPad Software, La Jolla, CA). All data were tested for normality using the Shapiro–Wilk test. All data were analyzed by unpaired *t*-test or one-way ANOVA, followed by the Tukey multiple comparisons test, where appropriate. For time courses, a two-way ANOVA with repeated measures was performed, followed by the Tukey multiple comparisons test. Differences were considered significant at $p < 0.05$.

Authors' Contributions

A.E.V., H.P., S.A.W., J.D.S., M.S.R., N.R.M., and W.J.A. designed the study and wrote the article. A.E.V., M.D.S., A.L., T.H., N.A.H., X.Y., and N.M. performed experiments and analyzed the data.

Author Disclosure Statement

S.A.W. has equity in Altamira Therapeutics Ltd. M.S.R. is a member of the Board of Directors at Eli Lilly and Company.

Funding Information

This work was supported by National Institutes of Health grants HL111664 and HL139842.

Supplementary Material

Supplementary Figure S1
Supplementary Figure S2
Supplementary Figure S3
Supplementary Figure S4
Supplementary Figure S5
Supplementary Figure S6
Supplementary Figure S7
Supplementary Figure S8

References

1. Ambasta RK, Schreiber JG, Janiszewski M, Busse R, and Brandes RP. Noxa1 is a central component of the smooth muscle NADPH oxidase in mice. *Free Radic Biol Med* 41: 193–201, 2006.
2. Ariazi EA, Taylor JC, Black MA, Nicolas E, Slifker MJ, Azzam DJ, and Boyd J. A new role for ERalpha: silencing via DNA methylation of basal, stem cell, and EMT genes. *Mol Cancer Res* 15: 152–164, 2017.
3. Baiardi G, Macova M, Armando I, Ando H, Tyurmin D, and Saavedra JM. Estrogen upregulates renal angiotensin II AT1 and AT2 receptors in the rat. *Regul Pept* 124: 7–17, 2005.
4. Balaban RS, Soltoff SP, Storey JM, and Mandel LJ. Improved renal cortical tubule suspension: spectrophotometric study of O2 delivery. *Am J Physiol* 238: F50–F59, 1980.
5. Barbaro NR, Foss JD, Kryshtal DO, Tsyba N, Kumaresan S, Xiao L, Mernaugh RL, Itani HA, Loperena R, Chen W, Dikalov S, Titze JM, Knollmann BC, Harrison DG, and Kirabo A. Dendritic cell amiloride-sensitive channels mediate sodium-induced inflammation and hypertension. *Cell Rep* 21: 1009–1020, 2017.
6. Beutler KT, Masilamani S, Turban S, Nielsen J, Brooks HL, Ageloff S, Fenton RA, Packer RK, and Knepper MA. Long-term regulation of ENaC expression in kidney by angiotensin II. *Hypertension* 41: 1143–1150, 2003.
7. Bhatia K, Elmarakby AA, El-Remessy AB, and Sullivan JC. Oxidative stress contributes to sex differences in angiotensin II-mediated hypertension in spontaneously hypertensive rats. *Am J Physiol Regul Integr Comp Physiol* 302: R274–R282, 2012.
8. Carlstrom M, Lai EY, Ma Z, Patzak A, Brown RD, and Persson AE. Role of NOX2 in the regulation of afferent arteriole responsiveness. *Am J Physiol Regul Integr Comp Physiol* 296: R72–R79, 2009.
9. Chabrashvili T, Kitiyakara C, Blau J, Karber A, Aslam S, Welch WJ, and Wilcox CS. Effects of ANG II type 1 and 2 receptors on oxidative stress, renal NADPH oxidase, and SOD expression. *Am J Physiol Regul Integr Comp Physiol* 285: R117–R124, 2003.
10. Chamberlin ME, LeFurgey A, and Mandel LJ. Suspension of medullary thick ascending limb tubules from the rabbit kidney. *Am J Physiol* 247: F955–F964, 1984.
11. Chen R, Sun W, Gu H, and Cheng Y. Aldosterone-induced expression of ENaC-alpha is associated with activity of p65/p50 in renal epithelial cells. *J Nephrol* 30: 73–79, 2017.
12. Cowley AW, Jr., Abe M, Mori T, O'Connor PM, Ohsaki Y, and Zheleznova NN. Reactive oxygen species as important determinants of medullary flow, sodium excretion, and hypertension. *Am J Physiol Renal Physiol* 308: F179–F197, 2015.
13. Dikalova A, Clempus R, Lassegue B, Cheng G, McCoy J, Dikalov S, San Martin A, Lyle A, Weber DS, Weiss D, Taylor WR, Schmidt HH, Owens GK, Lambeth JD, and Griendling KK. Nox1 overexpression potentiates angiotensin II-induced hypertension and vascular smooth muscle hypertrophy in transgenic mice. *Circulation* 112: 2668–2676, 2005.
14. Enslow BT, Stockand JD, and Berman JM. Liddle's syndrome mechanisms, diagnosis and management. *Integr Blood Press Control* 12: 13–22, 2019.
15. Frindt G and Palmer LG. Acute effects of aldosterone on the epithelial Na channel in rat kidney. *Am J Physiol Renal Physiol* 308: F572–F578, 2015.
16. Gavazzi G, Banfi B, Deffert C, Fiette L, Schappi M, Herrmann F, and Krause KH. Decreased blood pressure in NOX1-deficient mice. *FEBS Lett* 580: 497–504, 2006.
17. Gill PS and Wilcox CS. NADPH oxidases in the kidney. *Antioxid Redox Signal* 8: 1597–1607, 2006.
18. Gonzalez-Villalobos RA, Janjoulia T, Fletcher NK, Giani JF, Nguyen MT, Riquier-Brison AD, Seth DM, Fuchs S, Eladari D, Picard N, Bachmann S, Delpire E, Peti-Peterdi J, Navar LG, Bernstein KE, and McDonough AA. The absence of intrarenal ACE protects against hypertension. *J Clin Invest* 123: 2011–2023, 2013.
19. Gragasin FS, Xu Y, Arenas IA, Kainth N, and Davidge ST. Estrogen reduces angiotensin II-induced nitric oxide synthase and NAD(P)H oxidase expression in endothelial cells. *Arterioscler Thromb Vasc Biol* 23: 38–44, 2003.
20. Gray SP, Jha JC, Kennedy K, van Bommel E, Chew P, Szyndralewiez C, Touyz RM, Schmidt H, Cooper ME, and Jandeleit-Dahm KAM. Combined NOX1/4 inhibition with GKT137831 in mice provides dose-dependent reno- and atheroprotection even in established micro- and macrovascular disease. *Diabetologia* 60: 927–937, 2017.
21. Hilliard LM, Jones ES, Steckelings UM, Unger T, Widdop RE, and Denton KM. Sex-specific influence of angiotensin type 2 receptor stimulation on renal function: a novel therapeutic target for hypertension. *Hypertension* 59: 409–414, 2012.
22. Hwang AY, Dietrich E, Pepine CJ, and Smith SM. Resistant hypertension: mechanisms and treatment. *Curr Hypertens Rep* 19: 56, 2017.
23. Judd E and Calhoun DA. Management of hypertension in CKD: beyond the guidelines. *Adv Chronic Kidney Dis* 22: 116–122, 2015.
24. Kawada N, Imai E, Karber A, Welch WJ, and Wilcox CS. A mouse model of angiotensin II slow pressor response: role of oxidative stress. *J Am Soc Nephrol* 13: 2860–2868, 2002.
25. Kleyman TR, Kashlan OB, and Hughey RP. Epithelial Na(+) channel regulation by extracellular and intracellular factors. *Annu Rev Physiol* 80: 263–281, 2018.
26. Kopkan L, Castillo A, Navar LG, and Majid DS. Enhanced superoxide generation modulates renal function in ANG II-induced hypertensive rats. *Am J Physiol Renal Physiol* 290: F80–F86, 2006.
27. Laragh JH, Angers M, Kelly WG, and Lieberman S. Hypotensive agents and pressor substances. The effect of epinephrine, norepinephrine, angiotensin II, and others on

the secretory rate of aldosterone in man. *JAMA* 174: 234–240, 1960.
28. Lassegue B and Griendling KK. Reactive oxygen species in hypertension; an update. *Am J Hypertens* 17: 852–860, 2004.
29. Lassegue B, San Martin A, and Griendling KK. Biochemistry, physiology, and pathophysiology of NADPH oxidases in the cardiovascular system. *Circ Res* 110: 1364–1390, 2012.
30. Lozhkin A, Vendrov AE, Pan H, Wickline SA, Madamanchi NR, and Runge MS. NADPH oxidase 4 regulates vascular inflammation in aging and atherosclerosis. *J Mol Cell Cardiol* 102: 10–21, 2017.
31. Lu X, Wang F, Liu M, Yang KT, Nau A, Kohan DE, Reese V, Richardson RS, and Yang T. Activation of ENaC in collecting duct cells by prorenin and its receptor PRR: involvement of Nox4-derived hydrogen peroxide. *Am J Physiol Renal Physiol* 310: F1243–F1250, 2016.
32. Mamenko M, Zaika O, Ilatovskaya DV, Staruschenko A, and Pochynyuk O. Angiotensin II increases activity of the epithelial Na+ channel (ENaC) in distal nephron additively to aldosterone. *J Biol Chem* 287: 660–671, 2012.
33. Mamenko M, Zaika O, Prieto MC, Jensen VB, Doris PA, Navar LG, and Pochynyuk O. Chronic angiotensin II infusion drives extensive aldosterone-independent epithelial Na+ channel activation. *Hypertension* 62: 1111–1122, 2013.
34. Masilamani S, Kim GH, Mitchell C, Wade JB, and Knepper MA. Aldosterone-mediated regulation of ENaC alpha, beta, and gamma subunit proteins in rat kidney. *J Clin Invest* 104: R19–R23, 1999.
35. Matsuno K, Yamada H, Iwata K, Jin D, Katsuyama M, Matsuki M, Takai S, Yamanishi K, Miyazaki M, Matsubara H, and Yabe-Nishimura C. Nox1 is involved in angiotensin II-mediated hypertension: a study in Nox1-deficient mice. *Circulation* 112: 2677–2685, 2005.
36. McClintock SD, Attili D, Dame MK, Richter A, Silvestri SS, Berner MM, Bohm MS, Karpoff K, McCarthy CL, Spence JR, Varani J, and Aslam MN. Differentiation of human colon tissue in culture: effects of calcium on transepithelial electrical resistance and tissue cohesive properties. *PLoS One* 15: e0222058, 2020.
37. Mollnau H, Wendt M, Szocs K, Lassegue B, Schulz E, Oelze M, Li H, Bodenschatz M, August M, Kleschyov AL, Tsilimingas N, Walter U, Forstermann U, Meinertz T, Griendling K, and Munzel T. Effects of angiotensin II infusion on the expression and function of NAD(P)H oxidase and components of nitric oxide/cGMP signaling. *Circ Res* 90: E58–E65, 2002.
38. Muscella A, Aloisi F, Marsigliante S, and Levi G. Angiotensin II modulates the activity of Na+,K+-ATPase in cultured rat astrocytes via the AT1 receptor and protein kinase C-delta activation. *J Neurochem* 74: 1325–1331, 2000.
39. Nguyen Dinh Cat A, Montezano AC, Burger D, and Touyz RM. Angiotensin II, NADPH oxidase, and redox signaling in the vasculature. *Antioxid Redox Signal* 19: 1110–1120, 2013.
40. Nguyen MT, Lee DH, Delpire E, and McDonough AA. Differential regulation of Na+ transporters along nephron during ANG II-dependent hypertension: distal stimulation counteracted by proximal inhibition. *Am J Physiol Renal Physiol* 305: F510–F519, 2013.
41. Niu XL, Madamanchi NR, Vendrov AE, Tchivilev I, Rojas M, Madamanchi C, Brandes RP, Krause KH, Humphries J, Smith A, Burnand KG, and Runge MS. Nox activator 1: a potential target for modulation of vascular reactive oxygen species in atherosclerotic arteries. *Circulation* 121: 549–559, 2010.
42. Pechere-Bertschi A, Maillard M, Stalder H, Brunner HR, and Burnier M. Renal segmental tubular response to salt during the normal menstrual cycle. *Kidney Int* 61: 425–431, 2002.
43. Prieto MC, Reverte V, Mamenko M, Kuczeriszka M, Veiras LC, Rosales CB, McLellan M, Gentile O, Jensen VB, Ichihara A, McDonough AA, Pochynyuk OM, and Gonzalez AA. Collecting duct prorenin receptor knockout reduces renal function, increases sodium excretion, and mitigates renal responses in ANG II-induced hypertensive mice. *Am J Physiol Renal Physiol* 313: F1243–F1253, 2017.
44. Rajagopalan S, Kurz S, Munzel T, Tarpey M, Freeman BA, Griendling KK, and Harrison DG. Angiotensin II-mediated hypertension in the rat increases vascular superoxide production via membrane NADH/NADPH oxidase activation. Contribution to alterations of vasomotor tone. *J Clin Invest* 97: 1916–1923, 1996.
45. Sedeek M, Nasrallah R, Touyz RM, and Hebert RL. NADPH oxidases, reactive oxygen species, and the kidney: friend and foe. *J Am Soc Nephrol* 24: 1512–1518, 2013.
46. Stokes JB and Sigmund RD. Regulation of rENaC mRNA by dietary NaCl and steroids: organ, tissue, and steroid heterogeneity. *Am J Physiol* 274: C1699–C1707, 1998.
47. Stoos BA, Naray-Fejes-Toth A, Carretero OA, Ito S, and Fejes-Toth G. Characterization of a mouse cortical collecting duct cell line. *Kidney Int* 39: 1168–1175, 1991.
48. Sun P, Yue P, and Wang WH. Angiotensin II stimulates epithelial sodium channels in the cortical collecting duct of the rat kidney. *Am J Physiol Renal Physiol* 302: F679–F687, 2012.
49. Takeya R, Ueno N, Kami K, Taura M, Kohjima M, Izaki T, Nunoi H, and Sumimoto H. Novel human homologues of p47phox and p67phox participate in activation of superoxide-producing NADPH oxidases. *J Biol Chem* 278: 25234–25246, 2003.
50. Terryah ST, Fellner RC, Ahmad S, Moore PJ, Reidel B, Sesma JI, Kim CS, Garland AL, Scott DW, Sabater JR, Carpenter J, Randell SH, Kesimer M, Abraham WM, Arendshorst WJ, and Tarran R. Evaluation of a SPLUNC1-derived peptide for the treatment of cystic fibrosis lung disease. *Am J Physiol Lung Cell Mol Physiol* 314: L192–L205, 2018.
51. Thomas G, Xie D, Chen HY, Anderson AH, Appel LJ, Bodana S, Brecklin CS, Drawz P, Flack JM, Miller ER, 3rd, Steigerwalt SP, Townsend RR, Weir MR, Wright JT, Jr., Rahman M, and CRIC Study Investigators. Prevalence and prognostic significance of apparent treatment resistant hypertension in chronic kidney disease: report from the chronic renal insufficiency cohort study. *Hypertension* 67: 387–396, 2016.
52. Trott DW, Thabet SR, Kirabo A, Saleh MA, Itani H, Norlander AE, Wu J, Goldstein A, Arendshorst WJ, Madhur MS, Chen W, Li CI, Shyr Y, and Harrison DG. Oligoclonal CD8+ T cells play a critical role in the development of hypertension. *Hypertension* 64: 1108–1115, 2014.

53. Vendrov AE, Stevenson MD, Alahari S, Pan H, Wickline SA, Madamanchi NR, and Runge MS. Attenuated superoxide dismutase 2 activity induces atherosclerotic plaque instability during aging in hyperlipidemic mice. *J Am Heart Assoc* 6: e006775, 2017.
54. Vendrov AE, Sumida A, Canugovi C, Lozhkin A, Hayami T, Madamanchi NR, and Runge MS. NOXA1-dependent NADPH oxidase regulates redox signaling and phenotype of vascular smooth muscle cell during atherogenesis. *Redox Biol* 21: 101063, 2018.
55. Virani SS, Alonso A, Aparicio HJ, Benjamin EJ, Bittencourt MS, Callaway CW, Carson AP, Chamberlain AM, Cheng S, Delling FN, Elkind MSV, Evenson KR, Ferguson JF, Gupta DK, Khan SS, Kissela BM, Knutson KL, Lee CD, Lewis TT, Liu J, Loop MS, Lutsey PL, Ma J, Mackey J, Martin SS, Matchar DB, Mussolino ME, Navaneethan SD, Perak AM, Roth GA, Samad Z, Satou GM, Schroeder EB, Shah SH, Shay CM, Stokes A, VanWagner LB, Wang NY, Tsao CW, and American Heart Association Council on Epidemiology and Prevention Statistics Committee and Stroke Statistics Subcommittee. Heart disease and stroke statistics-2021 update: a report from the American Heart Association. *Circulation* 143: e254–e743, 2021.
56. Wang L, Wang X, Qu HY, Jiang S, Zhang J, Fu L, Buggs J, Pang B, Wei J, and Liu R. Role of kidneys in sex differences in angiotensin II-induced hypertension. *Hypertension* 70: 1219–1227, 2017.
57. Wei H, Mi X, Ji L, Yang L, Xia Q, Wei Y, Miyamori I, and Fan C. Protein kinase C-delta is involved in induction of NOX1 gene expression by aldosterone in rat vascular smooth muscle cells. *Biochemistry (Mosc)* 75: 304–309, 2010.
58. Wind S, Beuerlein K, Armitage ME, Taye A, Kumar AH, Janowitz D, Neff C, Shah AM, Wingler K, and Schmidt HH. Oxidative stress and endothelial dysfunction in aortas of aged spontaneously hypertensive rats by NOX1/2 is reversed by NADPH oxidase inhibition. *Hypertension* 56: 490–497, 2010.
59. Wingler K, Wunsch S, Kreutz R, Rothermund L, Paul M, and Schmidt HH. Upregulation of the vascular NAD(P)H-oxidase isoforms Nox1 and Nox4 by the renin-angiotensin system in vitro and in vivo. *Free Radic Biol Med* 31: 1456–1464, 2001.
60. Xue B, Pamidimukkala J, and Hay M. Sex differences in the development of angiotensin II-induced hypertension in conscious mice. *Am J Physiol Heart Circ Physiol* 288: H2177–H2184, 2005.
61. Yogi A, Mercure C, Touyz J, Callera GE, Montezano AC, Aranha AB, Tostes RC, Reudelhuber T, and Touyz RM. Renal redox-sensitive signaling, but not blood pressure, is attenuated by Nox1 knockout in angiotensin II-dependent chronic hypertension. *Hypertension* 51: 500–506, 2008.
62. Yu L, Bao HF, Self JL, Eaton DC, and Helms MN. Aldosterone-induced increases in superoxide production counters nitric oxide inhibition of epithelial Na channel activity in A6 distal nephron cells. *Am J Physiol Renal Physiol* 293: F1666–F1677, 2007.
63. Yusef YR, Thomas W, and Harvey BJ. Estrogen increases ENaC activity via PKCdelta signaling in renal cortical collecting duct cells. *Physiol Rep* 2: e12020, 2014.
64. Zeng SY, Yang L, Yan QJ, Gao L, Lu HQ, and Yan PK. Nox1/4 dual inhibitor GKT137831 attenuates hypertensive cardiac remodelling associating with the inhibition of ADAM17-dependent proinflammatory cytokines-induced signalling pathways in the rats with abdominal artery constriction. *Biomed Pharmacother* 109: 1907–1914, 2019.
65. Zhang J, Chandrashekar K, Lu Y, Duan Y, Qu P, Wei J, Juncos LA, and Liu R. Enhanced expression and activity of Nox2 and Nox4 in the macula densa in ANG II-induced hypertensive mice. *Am J Physiol Renal Physiol* 306: F344–F350, 2014.

Address correspondence to:
Dr. William J. Arendshorst
Department of Cell Biology and Physiology
University of North Carolina
6341 Medical Biomolecular Research Building
111 Mason Farm Road
Chapel Hill, NC 27599-7545
USA

E-mail: arends@med.unc.edu

Dr. Nageswara R. Madamanchi
Department of Internal Medicine
University of Michigan
7301A Medical Science Research Building III
1150 W. Medical Center Dr.
Ann Arbor, MI 48109-5644
USA

E-mail: madamanc@med.umich.edu

Date of first submission to ARS Central, March 17, 2021; date of final revised submission, September 28, 2021; date of acceptance, October 10, 2021.

Abbreviations Used

ACEi = angiotensin-converting enzyme inhibitors
ACTB = β-actin
AIH = Ang II-induced hypertension
Ang II = angiotensin II
ANOVA = analysis of variance
AQP1 = aquaporin 1
AQP2 = aquaporin 2
ARB = angiotensin receptor blockers
AT_1 = angiotensin II type 1
BP = blood pressure
BSA = bovine serum albumin
CD = collecting duct
CKD = chronic kidney disease
DHE = dihydroethidium
DMEM = Dulbecco's modified Eagle's medium
DPI = diphenyliodinium
ENaC = epithelial Na^+ channel
FBS = fetal bovine serum
HBSS = Hank's balanced salt solution
HTN = hypertension
L-NAME = L-Nitro arginine methyl ester
MRA = mineralocorticoid receptor antagonists
NAC = N-acetyl cysteine
NCC = Na-Cl cotransporter

Abbreviations Used (Cont.)

NCF2 = neutrophil cytosolic factor 2
NHE3 = Na-H exchanger 3
NKCC2 = Na-K-Cl cotransporter 2
NOX = NADPH oxidase
NOXA1 = NOX activator 1
OCLN = occludin
PBS = phosphate-buffered saline
PCR = polymerase chain reaction
PCT = proximal convoluted tubules
PEG-SOD = polyethylene glycol-conjugated superoxide dismutase
PKC = protein kinase C
RAAS = renin–angiotensin–aldosterone system
ROS = reactive oxygen species
sBP = systolic BP
siRNA = small-interfering RNA
TAL = thick ascending limb of loop of Henle
TUBB = β-tubulin
UNaV = urinary Na^+ excretion
VSMC = vascular smooth muscle cells